The all-seeing eye of resonant Auger electron spectroscopy: a study on aqueous KCl

Tsveta Miteva,[*,†] Nikolai V. Kryzhevoi,[‡] Nicolas Sisourat,[†] Christophe Nicolas,[¶] Wandared Pokapanich,[§] Thanit Saisopa,[‖] Prayoon Songsiriritthigul,[‖] Yuttakarn Rattanachai,[⊥] Andreas Dreuw,[#] Jan Wenzel,[#] Jérôme Palaudoux,[†] Gunnar Öhrwall,[@] Ralph Püttner,[△] Lorenz S. Cederbaum,[‡] Jean-Pascal Rueff,[†,¶] and Denis Céolin[*,¶]

†*Sorbonne Université, CNRS, Laboratoire de Chimie Physique Matière et Rayonnement, UMR 7614, F-75005 Paris, France*

‡*Theoretische Chemie, Physikalisch-Chemisches Institut, Universität Heidelberg, Im Neuenheimer Feld 229, D-69120 Heidelberg, Germany*

¶*Synchrotron SOLEIL, l'Orme des Merisiers, Saint-Aubin, F-91192 Gif-sur-Yvette Cedex, France*

§*Faculty of Science, Nakhon Phanom University, Nakhon Phanom 48000, Thailand*

‖*School of Physics, Suranaree University of Technology, Nakhon Ratchasima 30000, Thailand*

⊥*Department of Applied Physics, Faculty of Sciences and Liberal Arts, Rajamangala University of Technology Isan, Nakhon Ratchasima 30000, Thailand*

#*Interdisciplinary Center for Scientific Computing, Ruprecht-Karls University, Im Neuenheimer Feld 205A, D-69120 Heidelberg, Germany*

@*MAX IV Laboratory, Lund University, P.O. Box 118, SE-22100 Lund, Sweden*

△*Fachbereich Physik, Freie Universität Berlin, Arnimallee 14, D-14195, Berlin, Germany*

E-mail: tsveta.miteva@upmc.fr; denis.ceolin@synchrotron-soleil.fr

Methods

Experimental

For the present experiment we used the newly operational microjet setup that was specifically designed for the HAXPES station of the GALAXIES beamline[1,2]. A differentially-pumped tube in which the microjet head is inserted, is mounted on a 3-axes motorized manipulator in front of the spectrometer lens. Two holes of 2 mm diameter allow the photons to go in and out. At the end of the tube and in front of the lens, a 500 μm diameter hole skimmer allows the electrons created at the interaction point to go in the direction of the spectrometer. The microjet head is mostly composed of a 30 μm diameter vertical glass capillary facing a temperature-controlled catcher in CuBe having a 300 μm hole, and a camera. Piezo motors allow their precise alignment relative to each other and to the photon beam. The catcher is placed at a distance of about 5 mm from the capillary and is permanently pumped in order to extract the liquid. For the present experiment, a 0.5M KCl aqueous solution is injected in the capillary by a high performance liquid chromatography (HPLC) pump with a constant flux of 1.6 ml/min. The alignment of the setup is performed on the KCl aqueous solution by measuring the water O1s x-ray photoelectron peak intensity and by optimizing the liquid vs gas phase ratio. The pressure in the main chamber is kept below the 10^{-5} mbar range whereas it is kept at about 10^{-4} mbar in the differentially-pumped tube when the HPLC pump is ON. Our equipment is an updated version of the equipment used in Ref.[3] The aqueous potassium chloride solution was prepared by mixing >99% KCl salt with deionized water. Filtering and degazing procedures were systematically performed before injecting the solution. The spectrometer resolution of about 0.6 eV was achieved with the 500 eV pass energy and 0.5 mm slits. The photon energy resolution achieved at 2.8 keV and 3.6 keV was about 0.3 eV and 0.4 eV, respectively. The experimental 2D maps representing the evolution of the KLL Auger spectra in the vicinity of the Cl^- and K^+ K-edges, as a function of the photon energy, are shown in Figs. 2 and 3 in the main text, respectively. The aqueous

K^+ and Cl^- 1s ionization potentials were measured at $h\nu = 5\,keV$ and calibrated on the liquid contribution of the O1s XPS spectrum.[4] The maps were also calibrated using the O1s photoelectron line of liquid water but at photon energies close to the potassium and chloride 1s ionization thresholds.

Ab initio calculations

The theoretical X-ray absorption spectra were computed for the hexa-coordinated clusters of both ions, $K^+(H_2O)_6$ and $Cl^-(H_2O)_6$, which can be considered as representatives of the complete first solvation shell of the two ions[5–7]. The two structures shown in Fig. 4 were optimized at the DFT level of theory using the B3LYP functional and the 6-311++G(2d,2p) basis set[8,9]. The geometry optimization was performed with the Gaussian 09 package[10]. In order to obtain a realistic structure for K^+ corresponding to the bulk solution, we carried out constrained geometry optimization by choosing the equilibrium gas-phase geometries[11,12] belonging to the D_3 point group and then increasing the angle θ between the K-O bond and the C_3 axis to 55°. This angle was chosen such that the O-K-O angles are around the maxima of the angular distributions obtained from quantum mechanics/molecular mechanics simulations in Ref.[7]. Moreover, we fixed the K-O distance to 2.840 Å, such that it corresponds to the distances from other theoretical and experimental works[5–7].

The energies and transition moments of the core excited states of the bare ions and micro-solvated clusters were computed with the algebraic diagrammatic construction method for the polarization propagator[13] within the core-valence separation approximation[14–16] (CVS-ADC(2)x) as implemented in the Q-Chem package[17–20]. In the case of Cl^- the 6-311++G(3df,3pd) basis set[8,21] (excluding f functions) was used on all atoms, whereas in the case of K^+ we used the 6-311+G(2d,p) basis set[8,9] on all atoms, and two additional sets of s, p and d diffuse functions were added on K. The use of a smaller basis set in the case of K is due to the higher number of atomic orbitals compared to the case of Cl, and therefore, prohibitively high cost of the CVS-ADC(2)x computation. In our calculations the core space comprises the 1s or-

bital of K^+ or Cl^-, whereas the remaining occupied orbitals are included in the valence space. For the calculations of the XAS spectra we used the C_2 point group in the case of $K^+(H_2O)_6$ and $Cl^-(H_2O)_6$. To account for the lifetime broadening due to the Auger decay of the core excited states, we convolved the theoretical spectra with a Lorentzian function of FWHM 0.74 eV and 0.62 eV in the case of K^+ and Cl^-, respectively[22]. Additionally, we convolved the theoretical spectra with a Gaussian profile to also account for the experimental resolution (see Fig. 4 in the main text). We analyzed the core excited states by expanding the natural orbitals occupied by the excited electron (singly occupied natural orbitals, SONOs) ψ_i of the microsolvated clusters in the basis of SONOs of the bare K^+ or Cl^- ions, χ_{nl}

$$\psi_i = \sum_{nl} a^i_{nl} \chi_{nl} \tag{1}$$

where n and l stand for the principal and orbital quantum numbers as described in Ref.[23]. The expansion coefficients a^i_{nl} show the degree of delocalization of the excited electron and the mixing of the core excited states in the ligand field created by the surrounding water molecules (see Fig. 4).

The final states following KLL resonant Auger decay of $K^+(H_2O)_6$ and $Cl^-(H_2O)_6$ were computed at the Configuration Interaction Singles (CIS) level using the Graphical Unitary Group Approach (GUGA) as implemented in the GAMESS-US package[24–26]. In order to account for the relaxation effects upon core ionization, we employed a restricted open-shell Hartree-Fock reference wave function with a hole in the 2s orbital of both K^+ and Cl^-. We used the 6-311++G(2d,2p) basis set[8,9,21] on all atoms. Additionally, the basis set was augmented with two sets of s, p, d diffuse functions in the case of K^+, and three sets of s, p, d diffuse functions in the case of Cl^-. The larger basis set employed in the case of Cl was necessary in order to ensure the convergence of the excited states. The active space comprises the 2s and 2p orbitals of K/Cl with occupancy fixed to 6 and all virtual orbitals with occupancy fixed to 1. The remaining doubly occupied orbitals were frozen in the

calculation.[27]

PCI shift

In order to estimate the maximum amplitude of the PCI shift, we compare the positions of the normal KLL Auger lines of both Cl^-_{aq} and K^+_{aq} close to threshold with those recorded far from threshold, at photon energies $h\nu = 5\,keV$[28]. We observe a shift of $\sim$1 eV of the maxima towards lower kinetic energies as compared to the spectra reported in[28]. The magnitude of the shift is constant in the photon energy range of $\sim$8 eV above threshold and similar for the two ions. A possible explanation of the shift observed in our experiment is given in Ref.[29] where it was proposed that it is due to a process of internal ionization, i.e. excitation of the photoelectron into the conduction band, followed by normal Auger decay. The observed shift was explained as resulting from the PCI-like interaction between the Auger electron and the electron excited to the conduction band.

Core-excited states of Cl^-

The intensity of the $Cl^-(1s^{-1}4p)$ state is lower than that of the $Cl^-(1s^{-1}5p)$ state contrary to what is observed in K^+. This difference can be explained by the lower electron density of the 4p compared to the 5p electron in the region close to the core hole which thus results in the lower oscillator strength of the $1s^{-1}4p$ compared to the $1s^{-1}5p$ transition in Cl^- (see Fig. 1 in SI). In what follows we give a simple explanation of the difference in the radial density distributions of the $1s^{-1}4p$ and $1s^{-1}5p$ states in K^+ and Cl^-. In the case of K^+, the excited electron mainly sees a $2/r$ potential. In addition, it sees a short range potential originating from the point-like nucleus and the screening electrons. The influence of the latter can be described by a quantum defect $\delta \neq 0$, which is almost constant for the entire infinite Rydberg series. However, in case of Cl^- the outer electron does not experience a Coulomb potential and the short range potential becomes dominant. As a result of the absence of the Coulomb

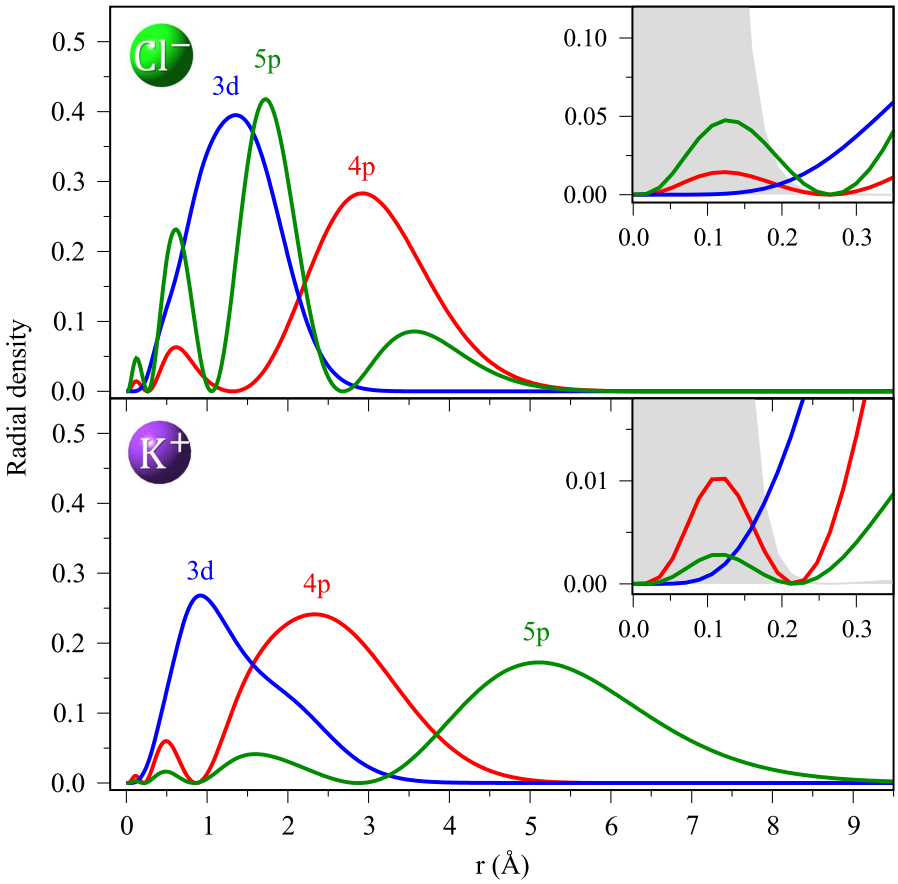

Figure SI 1: Radial density distributions of the singly-occupied natural orbital occupied by the excited electron corresponding to the $1s^{-1}4p$, $1s^{-1}3d$ and $1s^{-1}5p$ core excitations in K^+ (lower panel) and Cl^- (upper panel). The insets show the region of distances relevant for the overlap with the 1s core orbital whose radial density is shown as a grey shaded area.

potential we see a different behavior in the properties of the states, like e.g. only a finite number of bound states (here obviously 4p)[30]. In contrast to this, the 3d and 5p states are not bound.

In what follows we give a simple explanation of the difference in the radial density distributions of the $1s^{-1}4p$ and $1s^{-1}5p$ states in K^+ and Cl^-. In the case of K^+, the excited electron mainly sees a $2/r$ potential. In addition, it sees a short range potential originating from the point-like nucleus and the screening electrons. The influence of the latter can be described by a quantum defect $\delta \neq 0$, which is almost constant for the entire infinite Rydberg series. However, in case of Cl^- the outer electron does not experience a Coulomb potential and the short range potential becomes dominant. As a result of the absence of the Coulomb

potential we see a different behavior in the properties of the states, like e.g. only a finite number of bound states (here obviously 4p)[30]. In contrast to this, the 3d and 5p states are not bound.

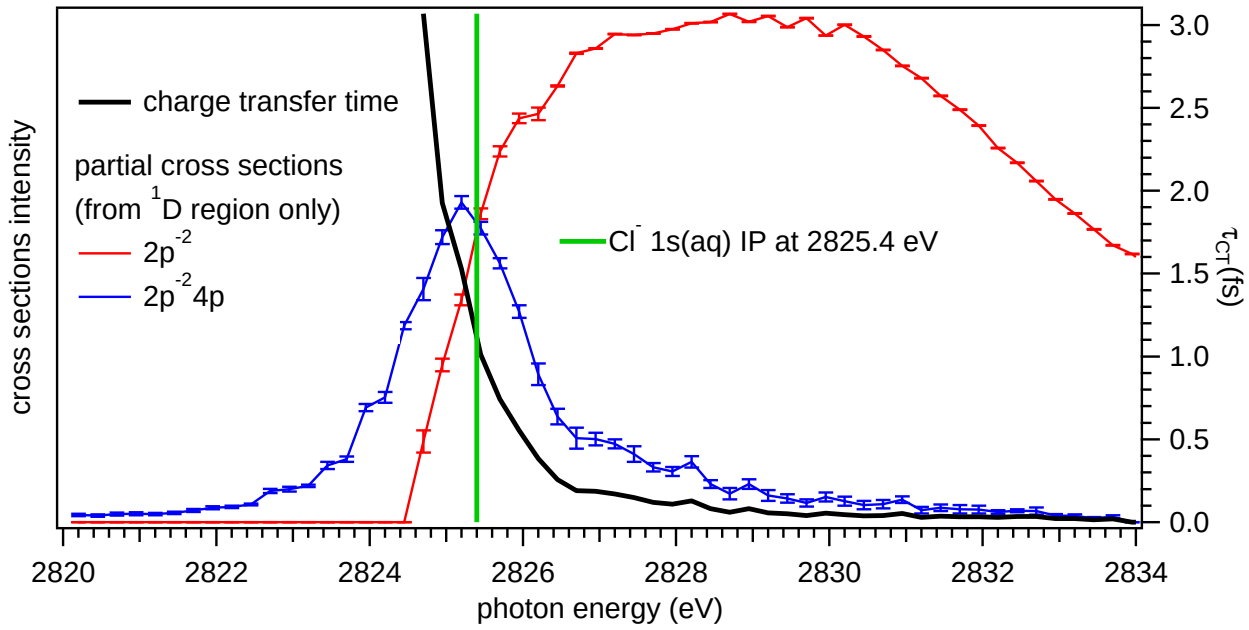

Figure SI 2: Partial cross sections and charge transfer time extracted from Fig. 3. The blue and red curves are obtained by integrating the area of the $2p^{-2}$ and $2p^{-2}4p$ final states (^{1}D state region only) at each photon energy step. From these curves we determine the charge transfer time τ_{CT} according to the formula $\tau_{CT} = \tau_c l/d$, with τ_c being the Cl 1s core-hole lifetime and l/d being the intensity ratio of the localized ($2p^{-2}4p$) and delocalized ($2p^{-2}$) states at a given excitation energy.[31] The green line defines the $Cl^-_{aq}(1s)$ ionization potential.

References

(1) Céolin, D.; Ablett, J.; Prieur, D.; Moreno, T.; Rueff, J.-P.; Marchenko, T.; Journel, L.; Guillemin, R.; Pilette, B.; Marin, T. et al. Hard X-ray photoelectron spectroscopy on the {GALAXIES} beamline at the {SOLEIL} synchrotron. *J. Electron Spectrosc. Relat. Phenom.* **2013**, *190, Part B*, 188 – 192.

(2) Rueff, J.-P.; Ablett, J. M.; Céolin, D.; Prieur, D.; Moreno, T.; Balédent, V.; Lassalle-Kaiser, B.; Rault, J. E.; Simon, M.; Shukla, A. The GALAXIES beamline at the

SOLEIL synchrotron: inelastic X-ray scattering and photoelectron spectroscopy in the hard X-ray range. *J. Synchrotron Rad.* **2015**, *22*, 175–179.

(3) Faubel, M.; Schlemmer, S.; Toennies, J. P. A molecular beam study of the evaporation of water from a liquid jet. *Z. Phys. D* **1988**, *10*, 269–277.

(4) Winter, B.; Faubel, M. Photoemission from Liquid Aqueous Solutions. *Chem. Rev.* **2006**, *106*, 1176–1211, PMID: 16608177.

(5) Ohtaki, H.; Radnai, T. Structure and dynamics of hydrated ions. *Chem. Rev.* **1993**, *93*, 1157–1204.

(6) Soper, A. K.; Weckström, K. Ion solvation and water structure in potassium halide aqueous solutions. *Biophys. Chem.* **2006**, *124*, 180 – 191.

(7) Ma, H. Hydration structure of Na^+, K^+, F^-, and Cl^- in ambient and supercritical water: A quantum mechanics/molecular mechanics study. *Int. J. Quant. Chem.* **2014**, *114*, 1006–1011.

(8) Krishnan, R.; Binkley, J. S.; Seeger, R.; Pople, J. A. SelfâĂŘconsistent molecular orbital methods. XX. A basis set for correlated wave functions. *J. Chem. Phys.* **1980**, *72*, 650–654.

(9) Blaudeau, J.-P.; McGrath, M. P.; Curtiss, L. A.; Radom, L. Extension of Gaussian-2 (G2) theory to molecules containing third-row atoms K and Ca. *J. Chem. Phys.* **1997**, *107*, 5016–5021.

(10) Frisch, M. J.; Trucks, G. W.; Schlegel, H. B.; Scuseria, G. E.; Robb, M. A.; Cheeseman, J. R.; Scalmani, G.; Barone, V.; Mennucci, B.; Petersson, G. A. et al. Gaussian 09 Revision D.01. Gaussian Inc. Wallingford CT 2009.

(11) Lee, H. M.; Kim, J.; Lee, S.; Mhin, B. J.; Kim, K. S. Aqua-potassium(I) complexes: Ab initio study. *J. Chem. Phys.* **1999**, *111*, 3995–4004.

(12) Lee, H. M.; Kim, D.; Kim, K. S. Structures, spectra, and electronic properties of halide-water pentamers and hexamers, $X^-(H_2O)_{5,6}$ (X=F,Cl,Br,I): Ab initio study. *J. Chem. Phys.* **2002**, *116*, 5509–5520.

(13) Schirmer, J. Beyond the random-phase approximation: A new approximation scheme for the polarization propagator. *Phys. Rev. A* **1982**, *26*, 2395–2416.

(14) Barth, A.; Schirmer, J. Theoretical core-level excitation spectra of N_2 and CO by a new polarisation propagator method. *J. Phys. B At. Mol. Opt. Phys.* **1985**, *18*, 867.

(15) Cederbaum, L. S.; Domcke, W.; Schirmer, J. Many-body theory of core holes. *Phys. Rev. A* **1980**, *22*, 206–222.

(16) Barth, A.; Cederbaum, L. S. Many-body theory of core-valence excitations. *Phys. Rev. A* **1981**, *23*, 1038–1061.

(17) Wenzel, J.; Wormit, M.; Dreuw, A. Calculating core-level excitations and x-ray absorption spectra of medium-sized closed-shell molecules with the algebraic-diagrammatic construction scheme for the polarization propagator. *J. Comp. Chem.* **2014**, *35*, 1900–1915.

(18) Wenzel, J.; Wormit, M.; Dreuw, A. Calculating X-ray Absorption Spectra of Open-Shell Molecules with the Unrestricted Algebraic-Diagrammatic Construction Scheme for the Polarization Propagator. *J. Chem. Theory Comput.* **2014**, *10*, 4583–4598.

(19) Wormit, M.; Rehn, D. R.; Harbach, P. H.; Wenzel, J.; Krauter, C. M.; Epifanovsky, E.; Dreuw, A. Investigating excited electronic states using the algebraic diagrammatic construction (ADC) approach of the polarisation propagator. *Mol. Phys.* **2014**, *112*, 774–784.

(20) Shao, Y.; Gan, Z.; Epifanovsky, E.; Gilbert, A. T.; Wormit, M.; Kussmann, J.; Lange, A. W.; Behn, A.; Deng, J.; Feng, X. et al. Advances in molecular quantum

chemistry contained in the Q-Chem 4 program package. *Mol. Phys.* **2015**, *113*, 184–215.

(21) McLean, A. D.; Chandler, G. S. Contracted Gaussian basis sets for molecular calculations. I. Second row atoms, Z=11âĂŞ18. *J. Chem. Phys.* **1980**, *72*, 5639–5648.

(22) Krause, M. O.; Oliver, J. H. Natural widths of atomic K and L levels, Kα X-ray lines and several KLL Auger lines. *J. Phys. Chem. Ref. Data* **1979**, *8*, 329–338.

(23) Miteva, T.; Wenzel, J.; Klaiman, S.; Dreuw, A.; Gokhberg, K. X-Ray absorption spectra of microsolvated metal cations. *Phys. Chem. Chem. Phys.* **2016**, *18*, 16671–16681.

(24) Brooks, B. R.; Laidig, W. D.; Saxe, P.; Handy, N. C.; Schaefer III, H. F. The Loop-Driven Graphical Unitary Group Approach: A Powerful Method for the Variational Description of Electron Correlation. *Phys. Scr.* **1980**, *21*, 312.

(25) Brooks, B. R.; Schaefer, H. F. The graphical unitary group approach to the electron correlation problem. Methods and preliminary applications. *J. Chem. Phys.* **1979**, *70*, 5092–5106.

(26) Schmidt, M. W.; Baldridge, K. K.; Boatz, J. A.; Elbert, S. T.; Gordon, M. S.; Jensen, J. H.; Koseki, S.; Matsunaga, N.; Nguyen, K. A.; Su, S. et al. General atomic and molecular electronic structure system. *J. Comp. Chem.* **1993**, *14*, 1347–1363.

(27) Mosnier, J.-P.; Kennedy, E. T.; van Kampen, P.; Cubaynes, D.; Guilbaud, S.; Sisourat, N.; Puglisi, A.; Carniato, S.; Bizau, J.-M. Inner-shell photoexcitations as probes of the molecular ions CH^+, OH^+, and SiH^+: Measurements and theory. *Phys. Rev. A* **2016**, *93*, 061401.

(28) Céolin, D.; Kryzhevoi, N. V.; Nicolas, C.; Pokapanich, W.; Choksakulporn, S.; Songsiriritthigul, P.; Saisopa, T.; Rattanachai, Y.; Utsumi, Y.; Palaudoux, J. et al.

Ultrafast Charge Transfer Processes Accompanying KLL Auger Decay in Aqueous KCl Solution. *Phys. Rev. Lett.* **2017**, *119*, 263003.

(29) Tchaplyguine, M.; Kivimäki, A.; Peredkov, S.; Sorensen, S. L.; Öhrwall, G.; Schulz, J.; Lundwall, M.; Rander, T.; Lindblad, A.; Rosso, A. et al. Localized versus delocalized excitations just above the 3d threshold in krypton clusters studied by Auger electron spectroscopy. *J. Chem. Phys.* **2007**, *127*, 124314.

(30) Buckman, S. J.; Clark, C. W. Atomic negative-ion resonances. *Rev. Mod. Phys.* **1994**, *66*, 539–655.

(31) Föhlisch, A.; Feulner, P.; Hennies, F.; Fink, A.; Menzel, D.; Sanchez-Portal, D.; Echenique, P. M.; Wurth, W. Direct observation of electron dynamics in the attosecond domain. *Nature* **2005**, *436*, 373.